Jiang, Y. and Chen, Q. 2003. "Buoyancy-driven single-sided natural ventilation in buildings with large openings," *International Journal of Heat and Mass Transfer*, 46(6), 973-988.

Buoyancy-Driven Single-Sided Natural Ventilation in Buildings with Large Openings

Yi Jiang[a] and Qingyan Chen[b,*]
[a] Building Technology Program, Massachusetts Institute of Technology
77 Massachusetts Avenue, Cambridge, MA 02139-4307
[b] School of Mechanical Engineering, Purdue University
1288 Mechanical Engineering Building, West Lafayette, IN 47907-1288

Abstract

Full-scale experimental and computational fluid dynamics (CFD) methods were used to investigate buoyancy-driven single-sided natural ventilation with large openings. Detailed airflow characteristics inside and outside of the room and the ventilation rate were measured. The experimental data were used to validate two CFD models: Reynolds averaged Navier-Stokes equation (RANS) modeling and large eddy simulation (LES). LES provides better results than the RANS modeling. With LES, the mechanism of single-sided ventilation was examined by turbulence statistical analysis. It is found that most energy is contained in low-frequency regions, and mean flow fields play an important role.

Keywords: computational fluid dynamics (CFD), large eddy simulation (LES), Reynolds averaged Navier-Stokes equation (RANS) modeling, experimental measurements, buoyancy-driven, single-sided natural ventilation

Nomenclature

A	opening area	$u^n_{j,k}$	instantaneous normal velocity at the opening at time t^n
C_d	discharge coefficient of openings	$U_{j,k}$	mean velocity normal to $x_j x_k$ plane
C_P	specific heat of air	V	air velocity
$C^e(t)$	the external concentration of the tracer gas at time t	V'	root-mean-square air velocity
$C^i(t)$	the internal concentration of the tracer gas at time t	V_{ref}	reference air velocity
g	gravity acceleration	w	the width of the opening
h	the height of the opening	W	total heat load within the room
h_j	subgrid-scale heat fluxes	x_i, x_j	coordinates in i and j-th directions
L	room volume	*Greek Symbols*	
$\dot{m}$	injection rate of the tracer gas	β	the expansion coefficient of air
N	total number of the time steps, during which $Q_{ins,T}$ is calculated	Δ_i	the filter width
		$\Delta\overline{P}_{open}$	the mean pressure difference across the opening

* Corresponding author. Tel.: 1-765-496-7562; Fax: 1-765-496-7534; Email: yanchen@purdue.edu

P	air pressure	$\Delta x_{ja}, \ldots$	the grid sizes in the x_j direction
$\overline{P}^e$	external mean air pressure	Δx_{jb}	within the opening
$\overline{P}^i$	internal mean air pressure	$\Delta x_{ka}, \ldots$	the grid sizes in the x_k direction
Pr	molecular Prandtl number	Δx_{kb}	within the opening
Q	ventilation rate	Δt^n	the time step size, $t^{n+1}-t^n$
$Q_{ins,T}$	the average instantaneous ventilation rate	ΔT	air temperature difference between T_{in} and T_{out}
Q_{mean}	mean ventilation rate	$\Delta T_{inlet-outlet}$	air temperature difference between the inlet and outlet openings
t	time	ν	air kinematic viscosity
$t_2 - t_1$	the time interval to integrate the internal concentration of tracer gas	ρ	air density
T	air temperature	σ_p^e	external root-mean-square pressure
T_{in}	inside air temperature	σ_p^i	internal root-mean-square pressure
T_{out}	outside air temperature	θ	air temperature
T_{ref}	reference air temperature	θ_0	reference air temperature
u_i, u_i	air velocity components in the x_i and x_j directions	τ_n	mean flow nominal time constant
		τ_{ij}	subgrid-scale Reynolds stresses

1. Introduction

Natural ventilation in buildings may create a comfortable and healthy indoor environment, and save energy compared to mechanical ventilation systems. In recent years, natural ventilation has attracted considerable interest from building designers [1, 2].

In a naturally ventilated building, air is driven in and out due to pressure differences produced by wind or buoyancy forces. There are three methods to study natural ventilation: empirical models, experimental measurements, and computational fluid dynamics (CFD) simulations. A "worst scenario" in natural ventilation arises on a warm and windless day, during which the ventilation is only driven by buoyancy forces. To study natural ventilation in such a condition, most designers use the empirical models. Although those models are simple and straightforward, they cannot account for the impacts of building forms, surroundings, and interior spaces on ventilation performances of a building. The experimental measurements and CFD simulations can predict these impacts. For example, Murakami et al. [3], Katayama et al. [4], Dascalaki [5], and Jiang and Chen [6] used these two methods to study wind-driven natural ventilation. The current investigation extends the study to buoyancy-driven natural ventilation.

Wind-tunnel and full-scale measurements are two commonly used experimental methods to provide detailed and reliable information about natural ventilation. Wind-tunnel tests are often used to study natural ventilation driven by wind forces. However, to study buoyancy-driven

ventilation, wind tunnels have difficulties generating high-Grashof number airflows analogous to a full-scale situation as required by a similarity theory. Therefore, a full-scale measurement is the choice. Since the study of natural ventilation driven only by buoyancy forces requires windless conditions, the outdoor environment should be controllable during the experiment. This investigation places a full-scale test room in a large laboratory environment so that the "outdoor environment" is windless. Nevertheless, the experimental measurement is an expensive method in terms of operation time and equipment costs.

CFD is an alternative approach to study natural ventilation in buildings. CFD is becoming popular due to its informative results and low labor and equipment costs. One of the CFD methods is large eddy simulation (LES), which solves three-dimensional, time-dependent airflow fields. Since one of the major driving forces in natural ventilation is wind, which changes its direction and magnitude over time, a transient simulation is required in such a study. LES can simulate transient airflows, and moreover, the detailed turbulence information provided by LES can be used for thermal comfort analysis. In recent years, LES has been successfully applied to airflows around buildings [7] and within buildings [8]. Since natural ventilation studies require correct prediction of both indoor and outdoor airflows, LES is an ideal candidate for natural ventilation studies.

Reynolds averaged Navier-Stokes equation (RANS) modeling is a popular CFD method and requires much less computing time than LES does. To study natural ventilation, however, it has some difficulties. First, RANS modeling cannot correctly predict airflows around and inside buildings as LES does [9, 10]. Second, as mentioned above, the unsteadiness caused by fluctuations in the wind-driven force requires a transient simulation. Some special methods have been used to add a time scale to RANS modeling, which results in a so-called unsteady RANS modeling [11, 12]. The unsteady RANS modeling still lacks the accuracy for detailed flow prediction and analysis as required by natural ventilation studies [13-17]. Since unsteady RANS modeling does not seem to be superior to regular RANS modeling and unsteady wind does not exist in the current buoyancy-driven natural ventilation case, this investigation will not consider the unsteady RANS modeling and only compare LES and the steady RANS modeling in terms of computing time and accuracy.

This paper will show the results of the experimental measurements, the steady RANS modeling, and LES for buoyancy-driven, single-sided natural ventilation with large openings and will compare the pros and cons of the methods. Two ventilation cases were studied: one with an open door and the other one with an open window.

2. Experimental measurements

This section will discuss the conducted experimental measurements, the impacts of the boundary conditions on the measurements, and a modified constant injection method for the ventilation rate measurement.

2.1 Description of the experimental setup

The experimental facility consists of two environmental chambers, a test chamber and an environmental chamber, placed in a large laboratory as shown in Fig. 1. The current study used only the test chamber to simulate an indoor environment and the laboratory space to simulate a windless outdoor environment. A 1,500 W baseboard heater was placed in the test chamber to generate buoyancy forces. The door of the test chamber was open to the laboratory. Therefore, a

single-sided ventilation driven by buoyancy forces was formed. When the lower half of the door was blocked, the situation turns into a room with an open "window."

The air velocity and temperature distributions were measured with six hot-sphere anemometers at different heights (0.1m, 0.5m, 0.9m, 1.3m, 1.7m, and 2.1m from the floor) in five different locations (P1 through P5) inside and outside of the test chamber as shown in Fig. 2. The anemometers have a great uncertainty if the air velocity is lower than 0.1 m/s, and the temperature measurement error is 0.3 K. The measurement frequency is 10 Hz. The experiment also used a tracer gas system to measure the ventilation rate of the room, and the type of the trace-gas was SF_6.

2.2 Impacts of the "outdoor" temperature variation on the measurements

The laboratory space outside of the test and environmental chambers was used to simulate a windless "outdoor" environment. However, the "outdoor" air temperature was not stable, and its temperature variation would affect the "indoor" temperature. This section discusses the impacts of this "outdoor" temperature variation on the measured results.

The measurements were performed in May and June 2001 in Greater Boston, Massachusetts, USA, during which the real outdoor air temperature varied significantly from day to day. Since Wall IV and the roof of the laboratory (Fig. 1) were exterior, their surface temperatures were affected directly by the weather. Since each measurement took eight hours, the temperature on those exterior surfaces and the laboratory air varied in different measurements. The surface temperatures varied as much as 3.5 K as shown in Table 1. However, when the measured air temperature and velocity were non-dimensionalized, the differences among the three door cases (the same indoor conditions but measured in three different days) were mostly within 5% as shown in Fig. 3. Therefore, the weather did not affect the non-dimensional results.

Fig. 3 also lists the measured results from the window case. Although the airflow distributions in the window case are very similar to those in the door case, there are three major differences. First, the temperature stratification outside of the room (at P1) in the window case is larger than that in the door case (Fig. 3 (a)). Second, the air velocity at the lower part of P2 in the window case is higher than that in the door case (Fig. 3 (b)). Third, the root-mean-square (RMS) velocities at the lower part of P2 and P3 in the window case are higher than those in the door case. These differences show that the airflow motion in the window case was stronger than that in the door case due to a larger temperature difference between inside and outside in the window case.

2.3 Tracer gas measurement

With a tracer gas system, several methods can be used to measure the ventilation rate of a building. The current investigation applied a constant injection method, in which the tracer gas, SF_6, was injected into the chamber at a constant rate, and the SF_6 concentration in the chamber was measured.

By assuming that the concentration of the tracer gas in the test chamber was uniform at all times and the SF_6 concentration from the laboratory air was very low, one can obtain the ventilation rate as [1]

$$Q = \frac{\dot{m}}{\frac{\int_{t_1}^{t_2} C^i(t)dt}{t_2 - t_1}} \quad (1)$$

Axley and Persily [18] pointed out that this constant injection method could provide accurate estimates of the mean ventilation rate regardless of the amplitude of the flow variation if the variation period of the flow field was small compared to the mean flow nominal time constant. The variation period of the flow field is the inverse of the peak frequency of the flow energy spectra, and the mean flow nominal time constant, τ_n, is defined as

$$\tau_n = \frac{V}{Q} \quad (2)$$

In the current investigation, τ_n was about 500 s, and the variation period of the flow field was about 10 s. Therefore, Eq. (1) gives accurate estimates of the mean ventilation rate. Because the flow fields studied in the current case were pseudo-steady, the SF_6 concentration and, consequently, the ventilation rate did not change over time.

Since the SF_6 concentration in the laboratory air was not very low, Eq. (1) must be modified. In the experiment, there was a time delay between the tracer gas entering the chamber and the tracer gas leaving the chamber. The delay was at the same order as the mean flow nominal time constant. Thus the modified formula to compute the ventilation rate becomes

$$Q = \frac{\dot{m}}{\frac{\int_{t_1}^{t_2} [C^i(t) - C^e(t - \tau_n)]dt}{t_2 - t_1}} \quad (3)$$

When the flow field reaches a steady state, $[C^i(t) - C^e(t - \tau_n)]$ will become constant. Since the Q and τ_n are unknown, they can be determined by solving Eqs. (2) and (3) together.

When using the constant injection method, the SF_6 concentration in the chamber was assumed to be uniform at all times, namely $C^i(t)$ does not vary with space. In reality, the SF_6 concentration may not be uniformly distributed and was measured at different locations. In Test 1, SF_6 concentration was measured at P2 through P5 at 1.7 m above the floor. Fig. 4 shows that the SF_6 concentrations are almost the same in the four indoor locations. In Tests 2, 3, and 4, SF_6 concentrations at 1.7 m from the floor in P4 and at 1.7 m from the floor at the opening were measured to represent the internal concentrations of SF_6. Since in Tests 2 and 4, there existed a difference of the concentrations between these two measured points, the ventilation rate was within a range instead of a single value. In all of these four tests, the SF_6 concentration of the entering air was measured at the lower part of the opening (0.3 m from the floor for the door case and 1.3 m from the floor for the window case). Based on the measured data and with Eqs. (2) and (3), one could obtain the ventilation rates as shown in Table 2. Table 2 shows that although the opening size of the window was only half of the door, the ventilation rate of the window case was more than half of that in the door case. This is mainly due to the stronger airflow motion in the window case than that in the door case as observed in Fig. 3.

3. Numerical methods

For the RANS modeling, the standard k-ε model [19] was used. Since the model is widely available from the literature, it will not be described here in detail. This section will briefly discuss the LES model, the numerical scheme, the required computing time, and the settings of objects.

By filtering the Navier-Stokes, continuity and energy equations, one would obtain the governing equations for LES as

$$\frac{\partial \overline{u_i}}{\partial t} + \frac{\partial}{\partial x_j}(\overline{u_i}\,\overline{u_j}) = -\frac{1}{\rho}\frac{\partial \overline{p}}{\partial x_i} + \nu\frac{\partial^2 \overline{u}_i}{\partial x_j \partial x_j} - \frac{\partial \tau_{ij}}{\partial x_j} + g_j\beta(\overline{\theta} - \theta_0)\delta_{ij} \tag{4}$$

$$\frac{\partial \overline{u_i}}{\partial x_i} = 0 \tag{5}$$

$$\frac{\partial \overline{\theta}}{\partial t} + \frac{\partial \overline{u}_j \overline{\theta}}{\partial x_j} = \frac{\partial}{\partial x_j}\left(\frac{\nu}{\mathrm{Pr}}\frac{\partial \overline{\theta}}{\partial x_j}\right) - \frac{\partial h_j}{\partial x_j} \tag{6}$$

where the bar represents grid filtering. The subgrid-scale Reynolds stresses in Eq. (4),

$$\tau_{ij} = \overline{u_i u_j} - \overline{u}_i \overline{u}_j \tag{7}$$

and the subgrid-scale heat fluxes in Eq. (6)

$$h_j = \overline{u_j \theta} - \overline{u}_j \overline{\theta} \tag{8}$$

are unknown and must be modeled with a subgrid-scale model. In this investigation, both of the Smagorinsky subgrid-scale (SS) model [20] and the filtered dynamic subgrid-scale (FDS) model [21] were used.

The present study used the simplified marker and cell method [22] to solve the governing equations of LES. A finite difference method was used to discretize the governing equations, and the standard second-order three-point central-differencing scheme to discretize the convection terms. The time term in the filtered Navier Stokes equations was discretized by the explicit Adams-Bashforth scheme.

The LES study used a non-uniform grid system. Since the Reynolds number was 40,000 and expected Kolmograph scale was about 10^{-4}, the smallest non-dimensional grid size was chosen as 0.03 m and the total grid number was 700,000. The time step size was 0.02 s. With this grid number and time step size, the simulation would require 10-day computing time on a workstation. For the RANS modeling, the non-uniform grid system was also applied. The grid number was less than half of that required by LES and the simulation only required 2-day computing time on a PC. Both CFD methods were tested for grid independence and further grid refinement yields only small and insignificant changes in the numerical results.

Since all the walls of the test chamber had a high thermal-resistance of 5.3 Km^2/W, they were simulated as adiabatic. The surface temperatures of the laboratory in Tests 3 and 4 were used as the boundary conditions for the door case and the window case, respectively. As

discussed previously, any set of surface temperatures of the laboratory could be used, since they would lead to the same conclusions.

4. Computational results and discussions

This section presents the numerical results for the door and window cases, such as the distributions of the air temperature and velocity and the ventilation rate of the room, as well as the discussions of the mechanism of single-sided ventilation.

4.1 The air distribution and ventilation rate

Fig. 5 compares the computed temperature profiles with the experimental data at the five positions for the door and window cases. In general, the computed results are in good agreement with the data. The LES models give slightly better results than the RANS modeling. The results show that within the chamber, the air temperature increases with height. But the temperature profile is not linearly distributed, and the largest temperature stratification occurs in the middle section of the room (0.9 m ~ 1.3 m from the floor),

LES can provide both mean and RMS air velocity. Although the RANS modeling can provide turbulence kinetic energy that is related to the RMS velocity, this kinetic energy cannot be converted to the RMS values of the air speed. Figs. 6 and 7 compare the computed mean and RMS air velocity with the corresponding measured data. For the door case, although the RANS modeling seems to perform better at the upper part of P2 than the LES models, it over-predicts the speeds at the bottom parts of P2, P3 and P4. The results obtained with the FDS model of the LES are in the best agreement with the experimental data in these regions. Nevertheless, the agreement in air velocity is not as good as that in air temperature. One possible reason is that the air velocity in this room was low (most regions were less than 0.1 m/s), which would affect the accuracy of the measurements. Figs. 6 and 7 also show that the high-speed regions are along top and bottom parts of the room. In the middle section, the air speeds are very low. This can explain why the temperature stratification in the middle section is very high (Fig. 5). It is because that there is not much air mixing in this part. Fig. 7 shows that the computed RMS velocity by LES is in reasonable agreement with the experimental data.

In the experiment, a small air current kit was used to observe the flow patterns in some particular areas. It was found that in the door case, a small recirculation region occurred at the upper right part of the room as shown in Fig. 8(a). Fig. 8(b) shows that the airflow pattern obtained with the FDS model provides a much clearer recirculation in the region than the RANS modeling. In an earlier study, Chen [23] found that the RANS modeling had difficulty predicting some secondary recirculations for indoor airflows.

The current experiment used a modified constant injection method to measure the ventilation rate. Based on the definition, the ventilation rate in the numerical simulations can be computed by integrating the velocity at the opening. There are two ways to do the integration. The first one is to extract the mean velocity, $U_{j,k}$, from a mean flow field, and compute the mean ventilation rate, Q_{mean} as

$$Q_{mean} = \frac{1}{2}\sum_{j=ja}^{jb}\sum_{k=ka}^{kb}\left|U_{j,k}\right|\Delta x_j \Delta x_k \qquad (9)$$

The other way is to determine the average instantaneous ventilation rate [10], $Q_{ins,T}$, over a time period of T as

$$Q_{ins,T} = \frac{\frac{1}{2}\sum_{n=1}^{N}\left(\sum_{j=ja}^{jb}\sum_{k=ka}^{kb}\left|u_{j,k}^{n}\right|\Delta x_j \Delta x_k\right)\cdot \Delta t^n}{\sum_{n=1}^{N}\Delta t^n} \tag{10}$$

Since the calculation of $Q_{ins,T}$ requires the transient flow field, only LES can provide it in the current study, and the steady RANS modeling cannot provide this value.

This investigation also used the semi-analytical method from Awbi [24] to calculate single-sided ventilation rate as a basis for comparison:

$$Q = \frac{C_d A}{3}\sqrt{gh\frac{\Delta T}{(T_{out}+273.15)}} \tag{11}$$

In Eq. (11), the discharge coefficient, C_d, depends on the characteristics of both the opening shape and the flow field. The current investigation set C_d as 0.61 (a value for a sharp-edged orifice). The ΔT is the temperature difference between the outdoor and indoor air. Although an energy balance equation

$$W = \rho Q C_p \Delta T_{inlet-outlet} \tag{12}$$

can give the temperature difference between the air at the inlet opening and the air at the outlet opening, $\Delta T_{inlet\text{-}outlet}$, it is not the same as ΔT. With the assumption of a linear temperature profile within the space, ΔT could be approximately as a half of $\Delta T_{inlet\text{-}outlet}$. Therefore,

$$W = 2\rho Q C_p \Delta T \tag{13}$$

By combining Eqs. (11) and (13), one can obtain the ventilation rate as

$$Q = h\left(\frac{WgC_D^2 w^2}{18\rho 8_P (T_{out}+273.15)}\right)^{1/3} \tag{14}$$

This equation suggests that the ventilation rate is proportional to the opening height, h. But the measured data show that the ventilation rate of the window case is more than half of that of the door case (Table 2). This incorrect conclusion drawn from Eq. (14) is due to the linear assumption of the temperature profile, which does not meet the real situation (Fig. 5). Therefore, the determination of the temperature difference, ΔT, is not a trivial issue, and a semi-analytical method may give wrong results. Nevertheless, the current investigation still used Eq. (14) to calculate the ventilation rate for a comparison with other methods.

Tables 3 and 4 show the ventilation rates computed with different methods. The LES results agree well with the experimental data. The RANS modeling gives much higher ventilation rates. The empirical model gives a reasonable estimation for the window case, but predicts a higher

value for the door case. Tables 3 and 4 also show that there is no significant difference between the mean ventilation rate and the average instantaneous ventilation rate. This is different from a wind-driven, single-sided ventilation, where the average instantaneous ventilation rate is much higher than the mean value, and the fluctuating flow field plays a more important role [10]. The following section will explain the reason through a statistical analysis.

4.2 Turbulence statistic analysis

Since LES calculates the mean and fluctuating pressure and velocity, it is possible to study the mechanism of single-sided ventilation through turbulence statistical analysis.

Fig. 9 shows the mean pressure distributions in the opening vicinity computed with the FDS model for the door and window cases. The higher internal pressure at the upper opening drives outflow and the lower internal pressure at the lower opening drives inflow. The neutral level is the height that separates the outflow and inflow. The mean pressure difference across the opening can be calculated with

$$\Delta \overline{P}_{open} = \frac{\int_0^h \left| \overline{P}^i - \overline{P}^e \right| dy}{2h} \tag{15}$$

Table 5 shows the computed mean pressure difference across the opening and the average internal and external RMS pressures. The internal pressure has a RMS value, σ_p^i, at the order of 10^{-3}, which is at the same order as that of the external wind RMS pressure acting on the opening, σ_p^e. While the mean pressure difference across the opening is at the order of 10^{-2}, which is almost ten times larger than the fluctuating pressure. Therefore, the mean flow field plays a more important role in this single-sided and buoyancy-driven natural ventilation. That is why the mean ventilation rate and the average instantaneous ventilation rate are almost the same.

Figs. 10 and 11 show the measured turbulence energy spectra of the air speed in the opening vicinity (at P1 and P2) for the door and window cases, respectively. The turbulence energy spectra of the air velocity remain almost the same when entering the room from outside or leaving the room from inside. This means that the airflow maintains its flow characteristics after going through the opening. The figures also show that the energy is mostly contained in the low-frequency region, less than 10^{-1} Hz, which has the characteristics of natural winds [25]. Ohba et al. [26] also pointed out that the energy of natural wind was contained in low-frequency region while the mechanical wind included small eddies in high-frequency regions.

Figs. 12 and 13 show the computed turbulence energy spectra with the FDS model of LES. The shapes of the spectra distributions are very similar to those from the measurements. Again, the energy is contained in low-frequency regions for both outside and inside air. The energy spectra distributions at the opening were also computed, which were not available from the measurements. For the door case (Fig. 12), the energy spectra at the lower part of the opening (H=0.5 m from the floor) are similar to those inside and outside of the room. At the upper part of the opening, however, the peak energy is shifted to the high-frequency region (close to 1 Hz). This is because that the sharp upper frame of the opening disturbs the flow field (Fig. 14(a)); thus, more energy is drawn from large eddies to small eddies. For the lower part, there is no obstacle blocking the airflow (Fig. 14(a)), the airflow enters the room smoothly, and most energy is still contained in low-frequency region. For the window case (Fig. 13), there are sharp frames at both of the lower and upper parts of the opening (Fig. 14(b)). The peak energy is shifted to a

high-frequency region at both parts (Fig. 13). The disturbances from the opening frame can be clearly observed in Fig. 14(b).

4.3 Discussions of the methods

Several methods have been used in the current investigation. Table 6 compares the pros and cons of those methods in terms of costs, available airflow information, and accuracy. The experimental method was the most reliable method. However, it is expensive by means of time and equipment costs and the obtained information is limited. Although the cost of the empirical model is almost zero, little information is available. Furthermore, the predicted ventilation rate could be wrong due to the simplification of the method. The steady RANS modeling requires less computing time than the LES, and it can provide detailed airflow field distribution. However, it is not as accurate as the LES method. Furthermore, the turbulence characteristics provided by the steady RANS modeling is limited, and they cannot be used for energy spectra analysis. The LES model seems to be a suitable tool to study natural ventilation by providing detailed and accurate airflow information with reasonable costs.

5. Conclusions

Single-sided natural ventilation driven by buoyancy forces was studied experimentally and numerically for a room with an open door or an open window.

The experiment used a full-scale test room with an opening to simulate an indoor environment, and placed the test room in a large laboratory space that simulated an “outdoor” environment. Some expensive measuring equipment, such as anemometers and a tracer-gas analyzer, were used to measure the distributions of air temperature and speed and ventilation rate. In the measurements, it took a long time to obtain the steady flow conditions. The control of “outdoor” environment is difficult due to the impacts from the real outdoor weather on the enclosure of the laboratory. Although the results from the experimental measurements are generally considered to be most reliable, it is difficult to measure the low air velocity. In the experiment, since the “outdoor” space was limited and the airflow distributions inside the room were not uniformly distributed, a modified constant injection method was developed to correctly predict the ventilation rate.

Between the two CFD models, the air temperature, air velocity, and ventilation rate predicted by the LES models are in better agreement with the measured data than those computed by the RANS modeling. An empirical model can give a reasonable estimation of the ventilation rate, provided that the discharge coefficient of the opening and the temperature difference between inside and outside air are correctly set up. However, correct prediction of the temperature difference is not easy, and the information obtained from the empirical model is limited. Based on the accuracy of the results and the equipment and labor costs, the FDS model of LES is more appropriate to study the current case. However, this paper investigated airflows with a simple geometry. To study the problems with a complex geometry or a large-scale site, LES has difficulty due to limitations of available memory and computing speed at present. So the RANS modeling would be a realistic choice in the near future. Furthermore, for an internal airflow study, the RANS modeling can produce reasonable results [27] with much less computing time than that required by LES, which makes the RANS modeling an obvious choice for this type of study.

With the mean and fluctuating pressures and velocities provided by LES, this investigation has studied the mechanism of single-sided ventilation with a turbulence statistical analysis. The

turbulence energy is mostly contained in low-frequency regions for both indoor and outdoor air. Local disturbances, such as a sharp geometry, could shift the energy to high-frequency regions. The magnitude of the fluctuating pressures close to the openings is much smaller than the mean pressure difference across the opening. Therefore, mean flow fields play a more important role in the buoyancy-driven, single-sided natural ventilation.

Acknowledgement

This work is supported by the U.S. National Science Foundation under grant CMS-9877118.

References

[1] D. Etheridge, M. Sandberg, Building ventilation: theory and measurement, John Wiley and Sons, Chichester; New York, 1996.
[2] F. Allard, Natural ventilation in buildings: a design handbook, James & James, London, UK. 1998.
[3] S. Murakami, S. Kato, S. Akabayashi, K. Mizutani, Y.D. Kim, Wind tunnel test on velocity-pressure field of cross-ventilation with open windows, ASHRAE Transactions 97 (1) (1991) 525-538.
[4] T. Katayama, J. Tsutsumi, A. Ishii, Full-scale measurements and wind tunnel tests on cross-ventilation, J. Wind Eng. Ind. Aerodyn. 41-44 (1992) 2553-2562.
[5] E. Dascalaki, M. Santamouris, A. Argiriou, C. Helmis, D. Asimakopoulos, K. Papadopoulos, A. Soilemes, On the combination of air velocity and flow measurements in single sided natural ventilation configurations, Energy and Buildings 24 (1996) 155-165.
[6] Y. Jiang, Q. Chen, Effect of fluctuating wind direction on cross natural ventilation in buildings from large eddy simulation, Building and Environment 37 (2002) 379-386.
[7] W. Rodi, J.H. Ferziger, M. Breuer and M. Pourquié, Status of large eddy simulation: results of a workshop, J. of Fluids Eng. 119 (1997) 248-262.
[8] S.J. Emmerich, K.B. McGrattan, Application of a large eddy simulation model to study room airflow, ASHRAE Transactions 104 (1998) 1128-1140.
[9] D. Lakehal, W. Rodi, Calculation of the flow past a surface-mounted cube with two-layer turbulence models, J. Wind Eng. Ind. Aerodyn. 67/68 (1997) 65-78.
[10] Y. Jiang, Q. Chen, Study of natural ventilation in buildings by large eddy simulation. J. Wind Eng. Ind. Aerodyn. 89 (13) (2001) 1155-1178.
[11] P.R. Spalart, S.R. Allmaras, A one-equation turbulence model for aerodynamic flows. La Recherche Aerospatiale, 1 (1) (1994) 5-21.
[12] P.A. Durbin, Separated flow computations with the k-ε-υ model. AIAA Journal, 33 (4) (1995) 659-664.
[13] L. Gianluca, P. Durbin, Unsteady 3D RANS simulations using the v^2-f model. Annual Research Briefs, Center for Turbulence Research, Stanford University, USA, 2000.
[14] M. Shur, P.R. Spalart, M. Strelets, A. Travin, Navier-Stokes simulationof shedding turbulent flow past a circular cylinder and a cylinder with a backward splitter plate. Third European CFD Conference, Paris, 1996.
[15] A. Travin, M. Shur, M. Strelets, P. Spalart, Detached-eddy simulations past a circular cylinder. Flow, Turbulence and Combustion, 63 (1-4) (2000) 293-313.
[16] P.R. Spalart, Strategies for turbulence modelling and simulations. International journal of heat and fluid flow, 21 (3) (2000) 252-263.

[17] A. Scotti, U. Piomelli, Turbulence models in pulsating flows. AIAA Journal, 40(3) (2002) 537-544.
[18] J. Axley, A. Persily, Integral mass balances and pulse injection tracer techniques, Report NISTIR 88-3855. U.S. Department of Commerce. National Institute of Standards and Technology, 1988.
[19] B.E. Launder, D.B. Spalding, The numerical computation of turbulent flows, Computer Methods in Applied Mechanics and Energy 3 (1974) 269-289.
[20] J. Smagorinsky, General circulation experiments with the primitive equations. I. The basic experiment, Monthly Weather Review 91 (1963) 99-164.
[21] W. Zhang, Q. Chen, Large eddy simulation of indoor airflow with a filtered dynamic subgrid scale model, International J. of Heat and Mass Transfer 43 (17) (2000) 3219-3231.
[22] F.H. Harlow, J.E. Welch, Numerical calculation of time-dependent viscous incompressible flow, Phys. Fluids 8 (12) (1965) 2182-2189.
[23] Q. Chen, Prediction of room air motion by Reynolds-stress models, Building and Environment 31 (3) (1996) 233-244.
[24] H.B. Awbi, Air movement in naturally-ventilated buildings. Department of Construction Management & Engineering, The University of Reading, WREC, 1996.
[25] Y. Zhu, Research on the fluctuant characteristics of natural wind and mechanical wind. Master Thesis, Department of Thermal Engineering, Tsinghua University, Beijing, P.R. China. (in Chinese), 2000.
[26] M. Ohba, K. Irie K., T. Kurabuchi, Study on airflow characteristics inside and outside a cross-ventilation model, and ventilation flow rates using wind tunnel experiments, J. Wind Eng. Ind. Aerodyn. 89 (2001) 1513-1524.
[27] X. Yuan, Q. Chen, L.R. Glicksman, Y. Hu, and X. Yang, Measurements and computations of room airflow with displacement ventilation, ASHRAE Transactions 105(1) (1999) 340-352.

Tables

Table 1 The surface temperatures of the laboratory (^{o}C).

Case Type	Door Case			Window Case
Test Number	Test 1	Test 2	Test 3	Test 4
Ceiling	25.11	23.11	26.67	26.46
Floor	22.78	22.11	24.78	24.28
Wall I	24.57	23.01	26.11	26.10
Wall II	24.39	22.83	25.58	25.47
Wall III	24.40	22.90	25.72	25.63
Wall IV	22.67	20.94	24.53	24.02

Table 2 The measured ventilation rates in the four tests.

Case Type	Door Case			Window Case
Test number	Test 1	Test 2	Test 3	Test 4
Ventilation rate (m^3/s)	0.107	0.102~0.140	0.127	0.075~0.088
Ventilation rate (ACH)	9.63	9.18~12.60	11.43	6.75~7.92

Table 3 Air exchange rate for the door case.

	Experimental	Empirical	RANS (k-ε)	LES (FDS model)	LES (SS model)

	measurement	model		Q_{ins}/L	Q_{mean}/L	Q_{ins}/L	Q_{mean}/L
ACH	9.18-12.6	13.6	15.2	10.6	10.5	10.4	10.2

Table 4 Air exchange rate for the window case.

	Experimental measurement	Empirical model	RANS (k-ε) Q_{mean}/L	LES (FDS model)		LES (SS model)	
				Q_{ins}/L	Q_{mean}/L	Q_{ins}/L	Q_{mean}/L
ACH	6.75~7.92	6.8	8.55	6.97	6.96	6.73	6.72

Table 5 The computed mean and RMS pressure distributions across the opening.

Door Case			Window Case		
$\Delta\overline{P}_{open}$ (Pa)	σ_p^i (Pa)	σ_p^e (Pa)	$\Delta\overline{P}_{open}$ (Pa)	σ_p^i (Pa)	σ_p^e (Pa)
0.012	0.0012	0.0019	0.022	0.0027	0.0033

Table 6 Comparison among different methods to study buoyancy-driven single-sided ventilation.

	Time Cost	Equipment cost	Flow field distribution	Ventilation rate	Statistical analysis
Experiment	Highest	Highest	Limited	Accurate	Limited
Empirical	Low	Low	Little	Not accurate	No
RANS (steady)	Middle	Middle	Detailed but not accurate.	Not accurate	Limited
LES	High	Middle	Detailed and accurate.	Accurate	Detailed.

Figure Captions

Fig. 1 The configuration of the laboratory.
(a) The plan of the laboratory (b) A-A section
Fig. 2 The measuring positions.
Fig. 3 Measured airflow distributions at the five locations (Non-dimensional values). Circles: Test 1; Squares: Test 2; Deltas: Test 3; Black dots with dashed lines: Test 4.
(a) Mean air temperature profiles (b) Mean air velocity profiles
(c) Root-mean-square (RMS) velocity profiles
Fig. 4 The measured SF_6 at 1.7 m above the floor in P2 through P5 and 0.3 m above the floor in the opening for Test 1.
Fig.5 Comparison of the computed temperature profiles with the measured data at the five positions in and around the chamber with an open door or window. Circles: Experimental data; Solid lines: the SS model; Dashed lines: the FDS model; Dash-dot lines: the RANS modeling.
(a) Door Case (b) Window Case
Fig. 6 Comparison of the computed mean air velocity profiles with the measured data at the five positions in and around the chamber with an open door or window. Circles: Experimental data; Solid lines: the SS model; Dashed lines: the FDS model; Dash-dot lines: the RANS modeling.
(a) Door Case (b) Window Case
Fig. 7 Comparison of the computed RMS velocity profiles with the measured data at the five positions in and around the chamber with an open door or window. Circles: Experimental data; Solid lines: the SS model; Dash-dot lines: the FDS model.

(a) Door Case (b) Window Case

Fig. 8 Comparison of observed and computed airflow pattern along the section at P1, P2, P3, and P5.

(a) The airflow pattern observed.

(b) The airflow pattern computed by RANS and LES with FDS.

Fig. 9 Distributions of mean pressure in the vicinity of the opening. Solid lines: internal pressure (0.06 m from the opening); Dashed lines: external pressure (0.06 m from the opening).

(a) Door Case (b) Window Case

Fig. 10 The measured turbulence energy spectra in the opening vicinity for the open door case.

(a) H=0.5 m from the floor at P1. (b) H=0.5 m from the floor at P2.

(c) H=1.7 m from the floor at P1. (d) H=1.7 m from the floor at P2.

Fig. 11 The measured turbulence energy spectra in the opening vicinity for the open window case.

(a) H=0.5 m from the floor at P1. (b) H=0.5 m from the floor at P2.

(c) H=1.7 m from the floor at P1. (d) H=1.7 m from the floor at P2.

Fig. 12 The computed turbulence energy spectra in the opening vicinity for the open door case. Solid lines: P1 (outside of the room); Dashed lines: P2 (inside of the room); Dotted lines: at the opening.

(a) H=0.5 m from the floor (b) H=1.7 m from the floor

Fig. 13 The computed turbulence energy spectra in the opening vicinity for the open window case. Solid lines: P1 (outside of the room); Dashed lines: P2 (inside of the room); Dotted lines: at the opening.

(a) H=1.3 m from the floor (b) H=1.7 m from the floor

Fig. 14 The mean air velocity distribution at the opening vicinity.

(a) Open door case (b) Open window case

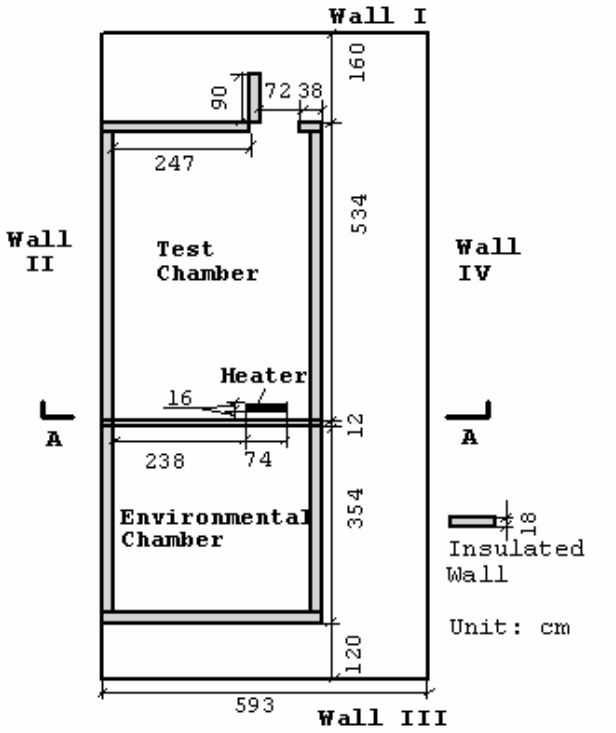

(a) The plan of the laboratory

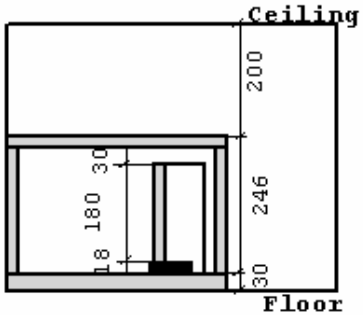

(b) A-A section

Fig. 1 The configuration of the laboratory.

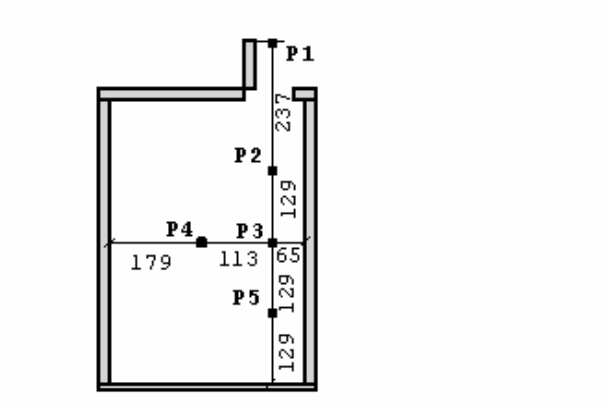

Fig. 2 The measuring positions.

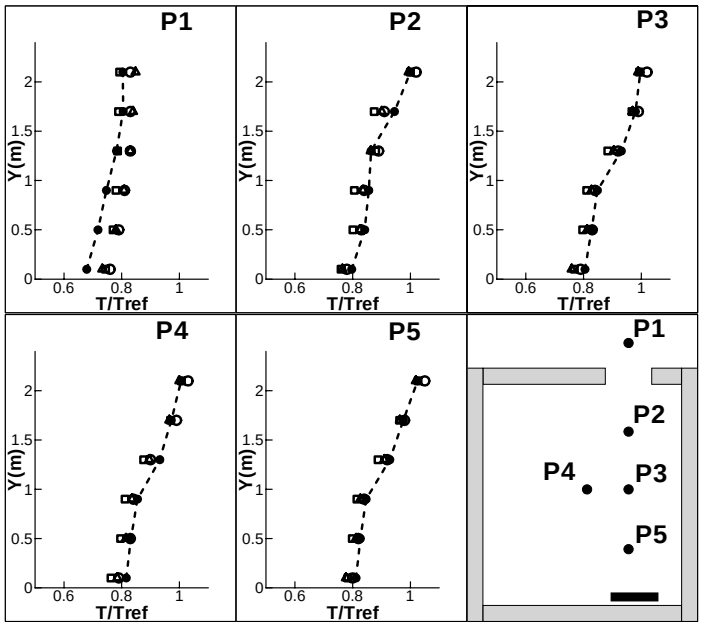

(a) Mean air temperature profiles

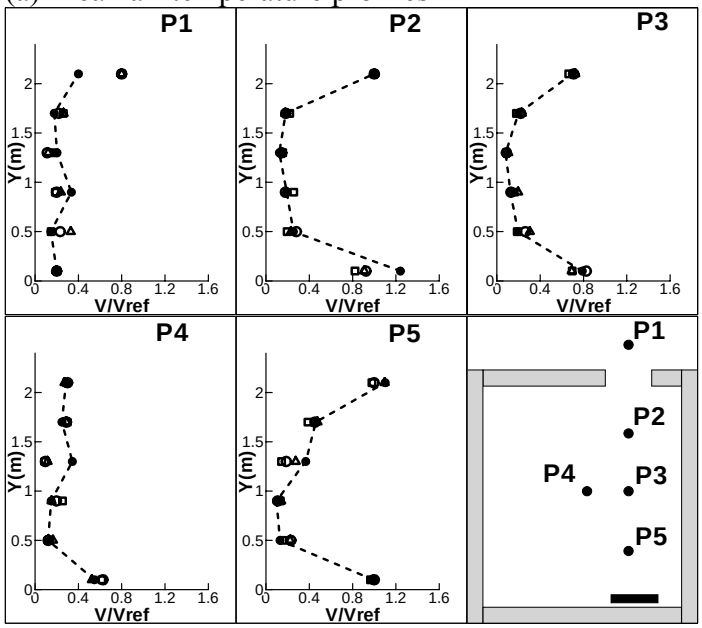

(b) Mean air velocity profiles

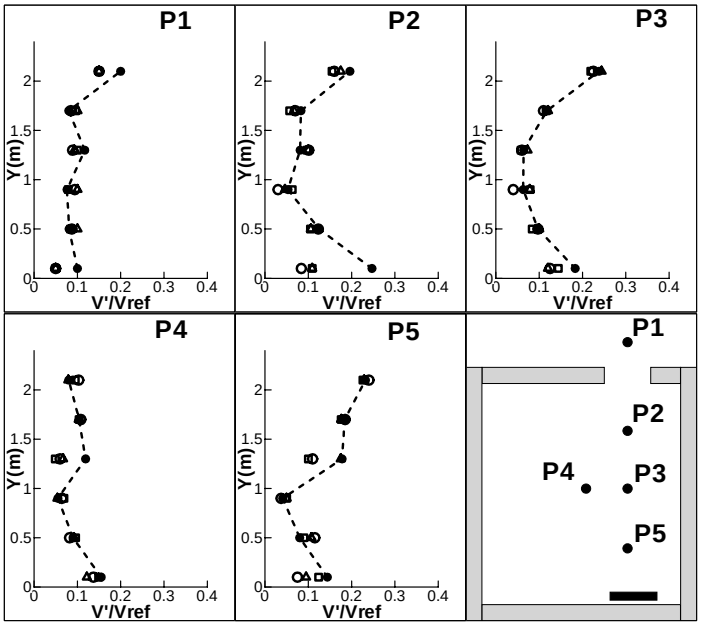

(c) Root-mean-square (RMS) velocity profiles

Fig. 3 Measured airflow distributions at the five locations (Non-dimensional values). Circles: Test 1; Squares: Test 2; Deltas: Test 3; Black dots with dashed lines: Test 4.

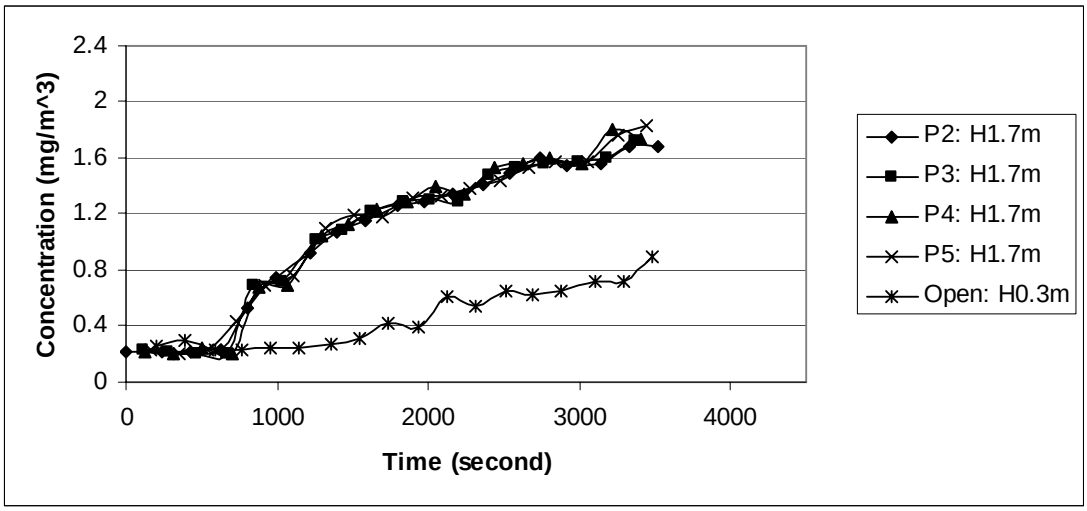

Fig. 4 The measured SF_6 at 1.7 m above the floor in P2 through P5 and 0.3 m above the floor in the opening for Test 1.

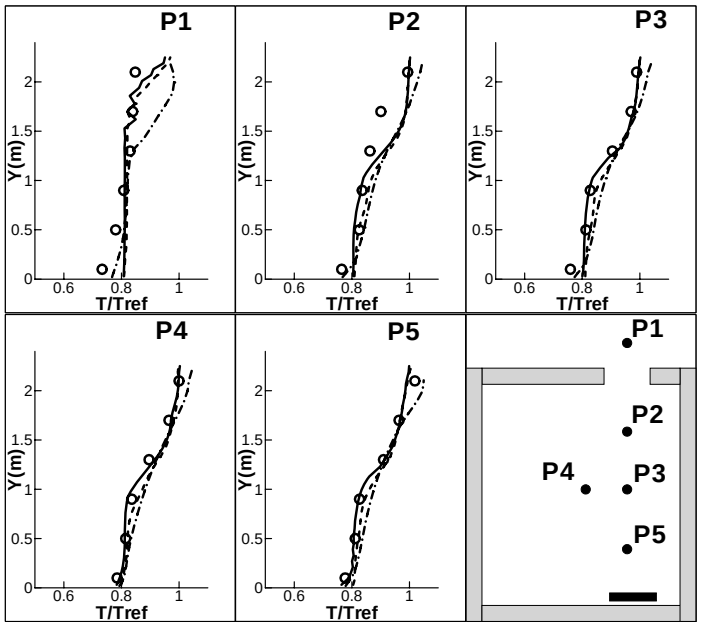

(a) Door Case

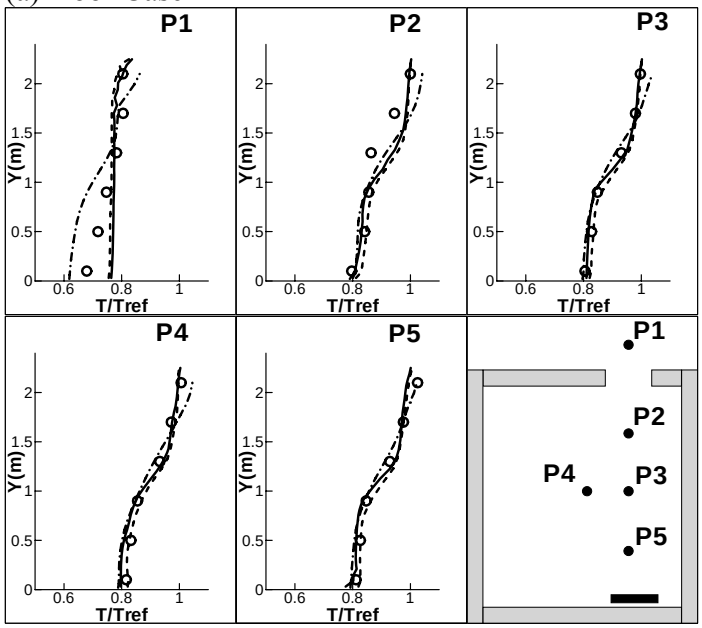

(b) Window Case

Fig.5 Comparison of the computed temperature profiles with the measured data at the five positions in and around the chamber with an open door or window. Circles: Experimental data; Solid lines: the SS model; Dashed lines: the FDS model; Dash-dot lines: the RANS modeling.

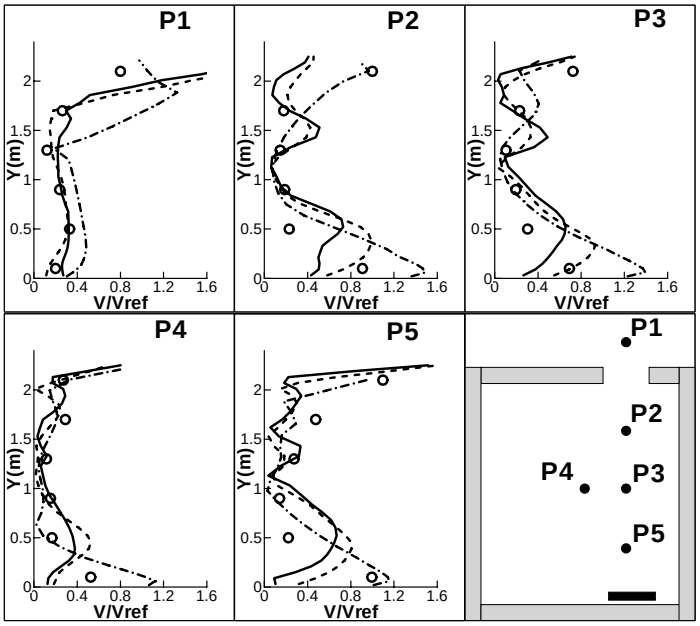

(a) Door Case

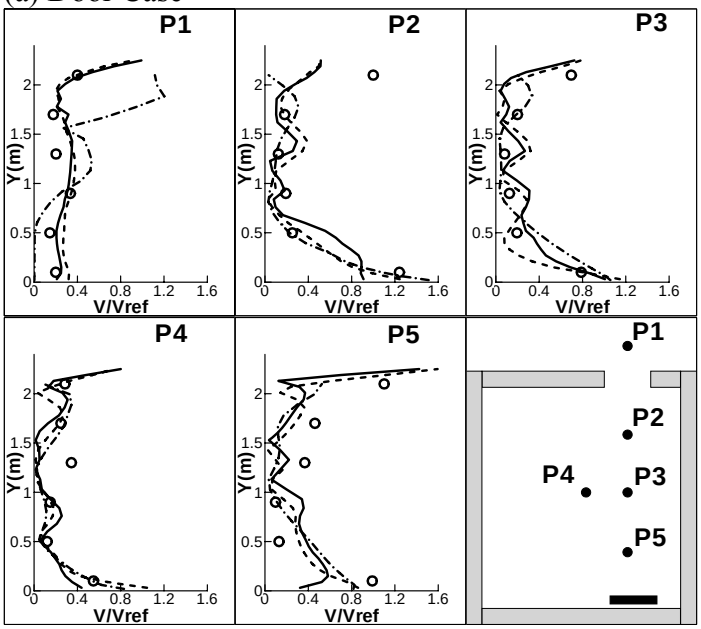

(b) Window Case

Fig. 6 Comparison of the computed mean air velocity profiles with the measured data at the five positions in and around the chamber with an open door or window. Circles: Experimental data; Solid lines: the SS model; Dashed lines: the FDS model; Dash-dot lines: the RANS modeling.

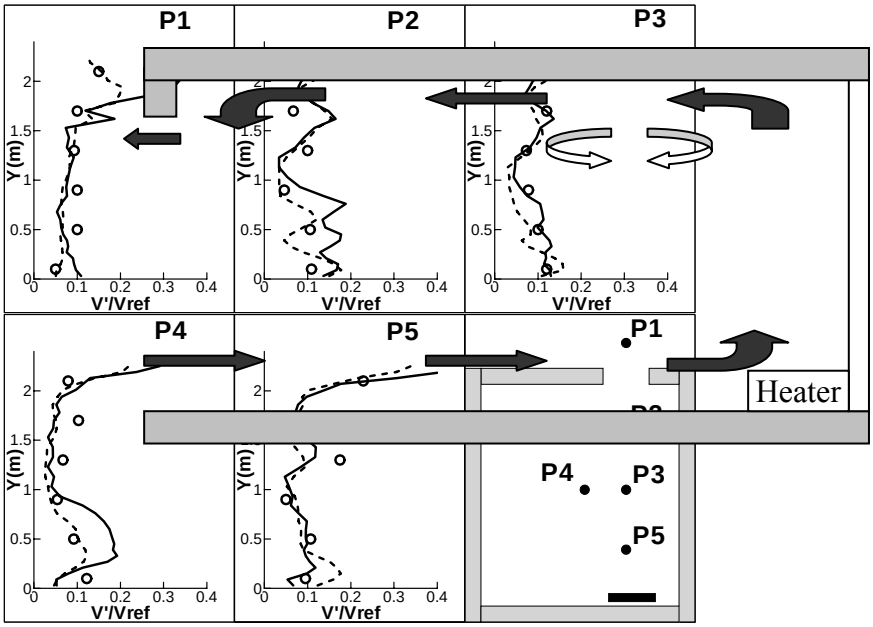

(a) Door Case

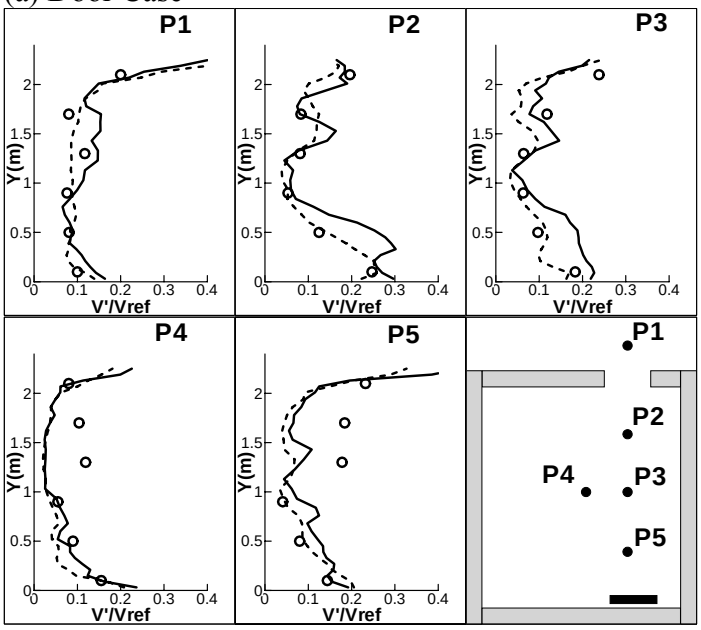

(b) Window case

Fig. 7 Comparison of the computed RMS velocity profiles with the measured data at the five positions in and around the chamber with an open door or window. Circles: Experimental data; Solid lines: the SS model; Dash-dot lines: the FDS model.

(a) The airflow pattern observed.

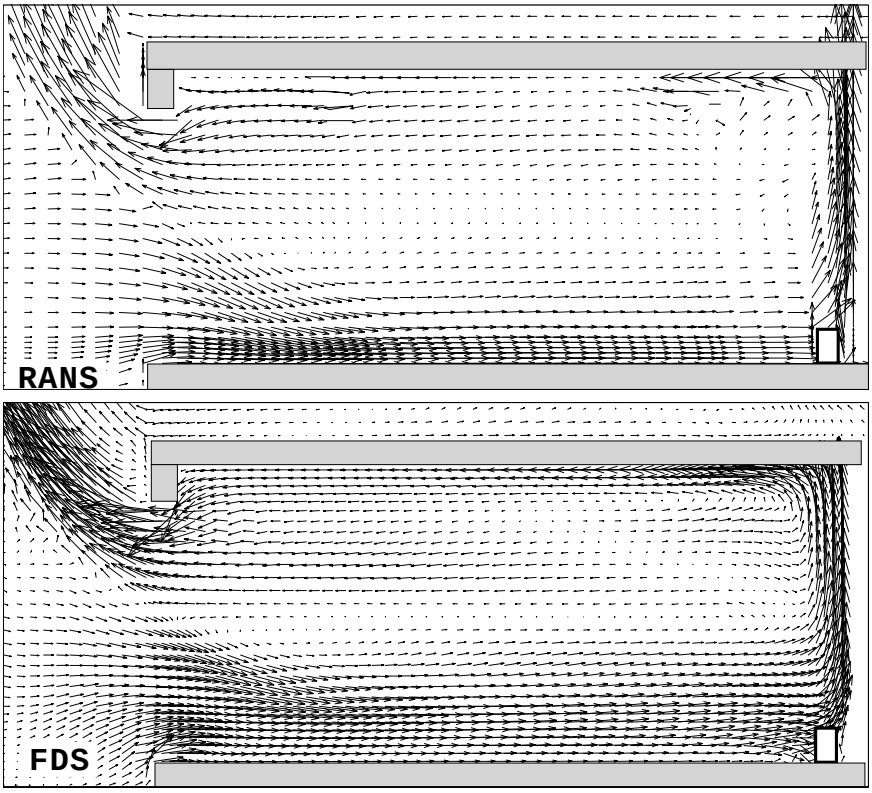

(b) The airflow pattern computed by RANS and LES with FDS.

Fig. 8 Comparison of observed and computed airflow pattern along the section at P1, P2, P3, and P5.

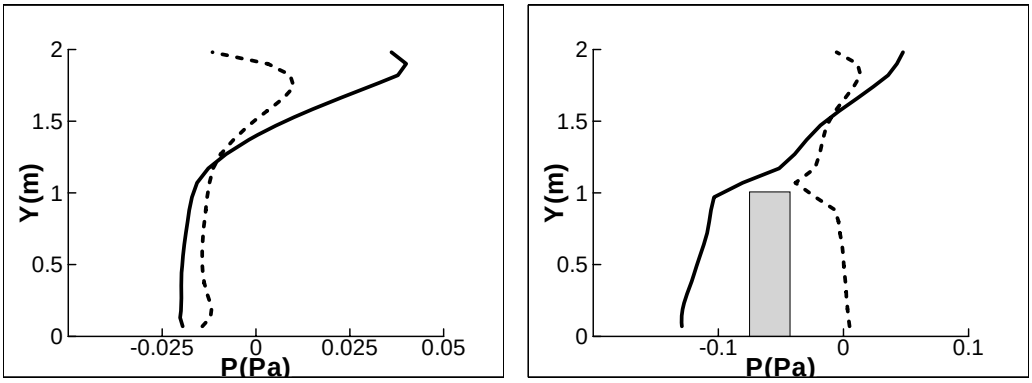

(a) Door case (b) Window case

Fig. 9 Distributions of mean pressure in the vicinity of the opening. Solid lines: internal pressure (0.06 m from the opening); Dashed lines: external pressure (0.06 m from the opening).

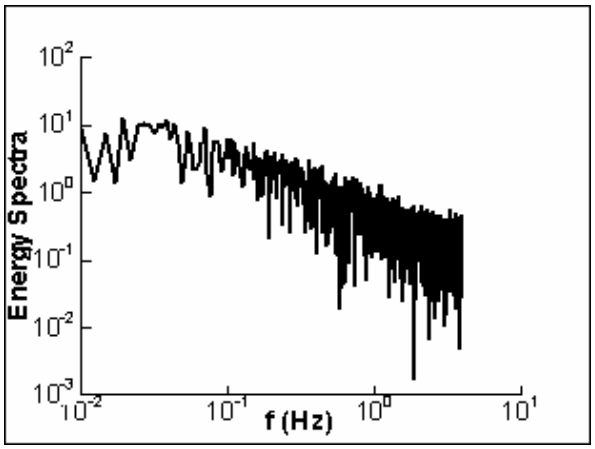

(a) H=0.5 m from the floor at P1.

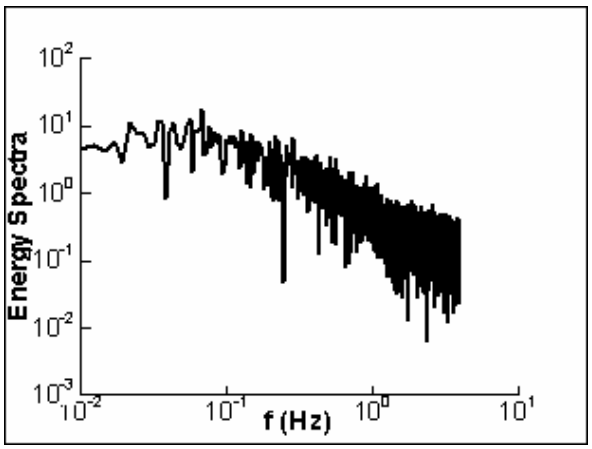

(b) H=0.5 m from the floor at P2.

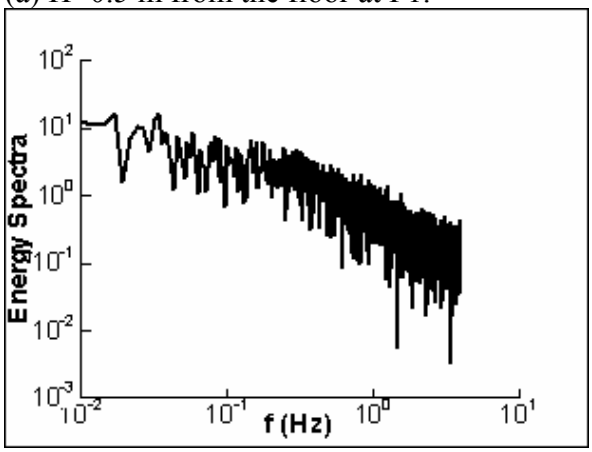

(c) H=1.7 m from the floor at P1.

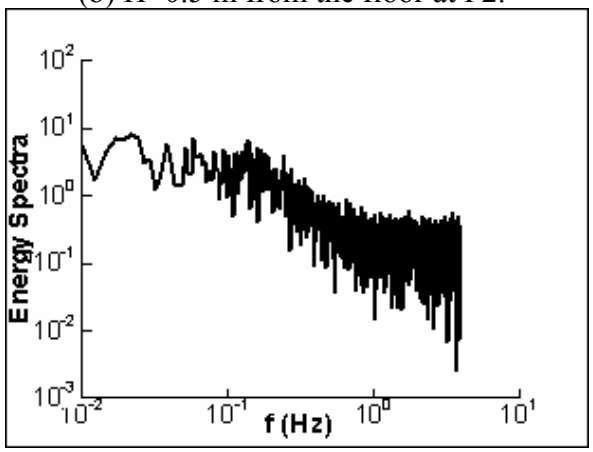

(d) H=1.7 m from the floor at P2.

Fig. 10 The measured turbulence energy spectra in the opening vicinity for the open door case.

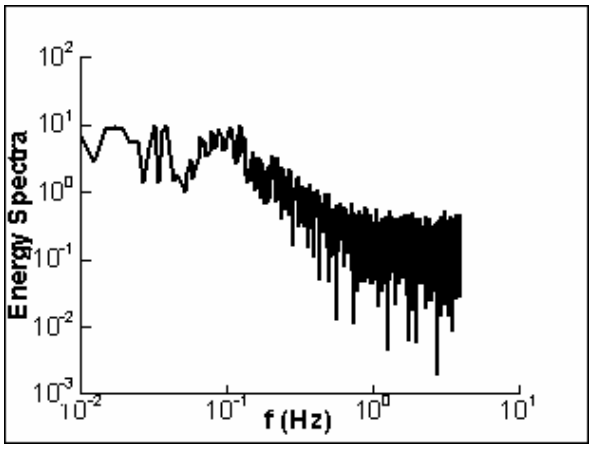

(a) H=0.5 m from the floor at P1.

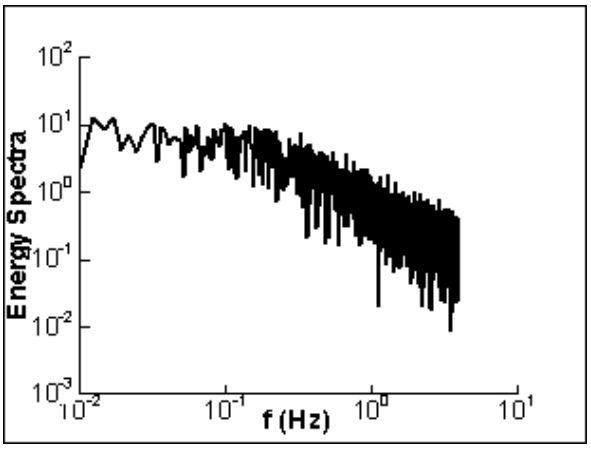

(b) H=0.5 m from the floor at P2.

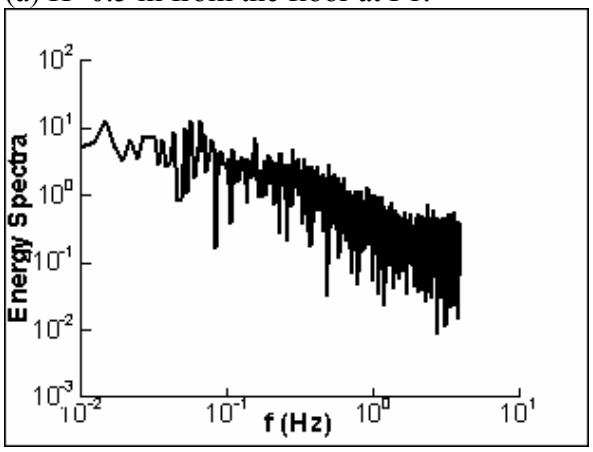

(c) H=1.7 m from the floor at P1.

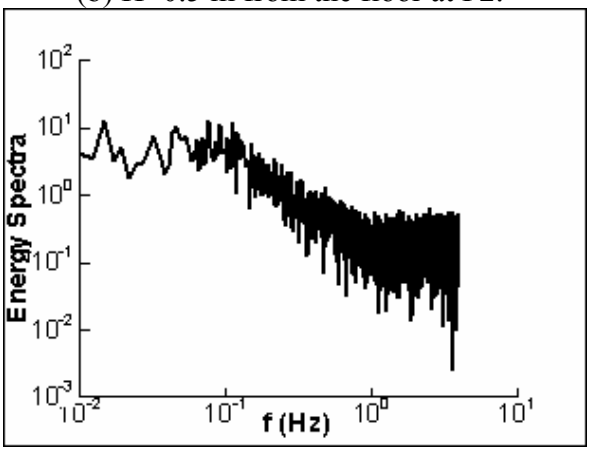

(d) H=1.7 m from the floor at P2.

Fig. 11 The measured turbulence energy spectra in the opening vicinity for the open window case.

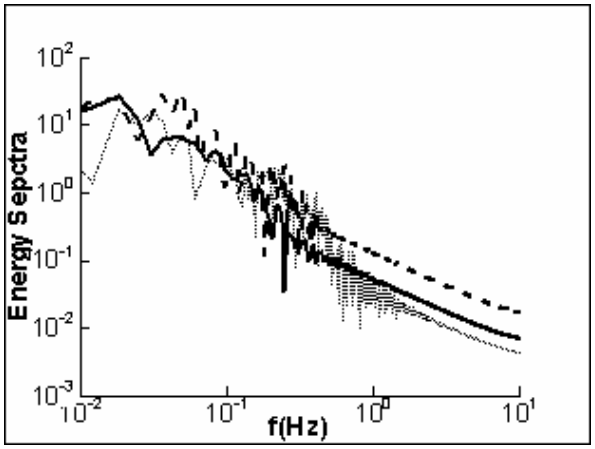

(a) H=0.5 m from the floor

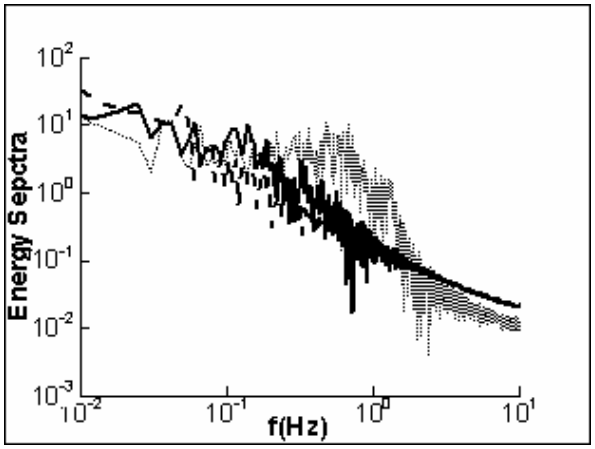

(b) H=1.7 m from the floor

Fig. 12 The computed turbulence energy spectra in the opening vicinity for the open door case. Solid lines: P1 (outside of the room); Dashed lines: P2 (inside of the room); Dotted lines: at the opening.

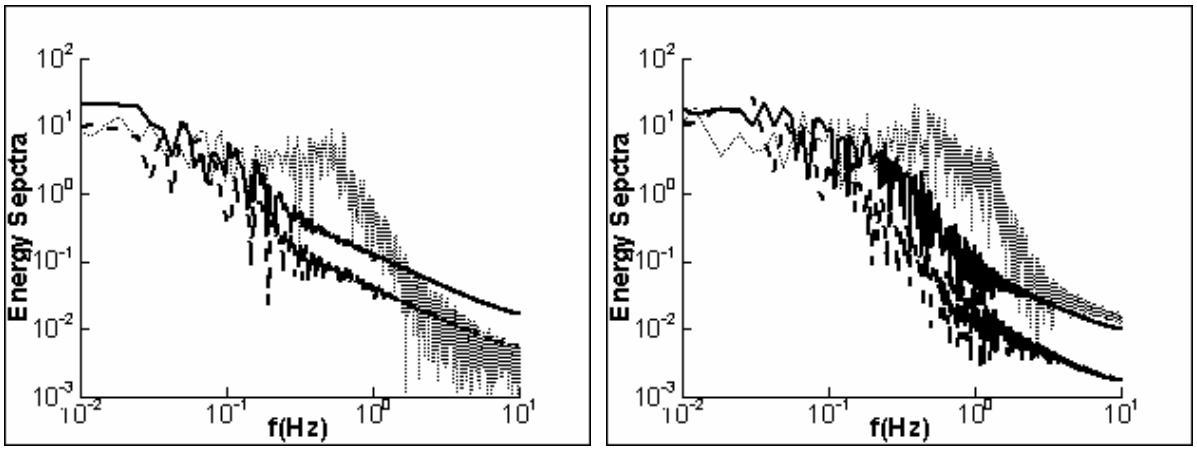

(a) H=1.3 m from the floor (b) H=1.7 m from the floor

Fig. 13 The computed turbulence energy spectra in the opening vicinity for the open window case. Solid lines: P1 (outside of the room); Dashed lines: P2 (inside of the room); Dotted lines: at the opening.

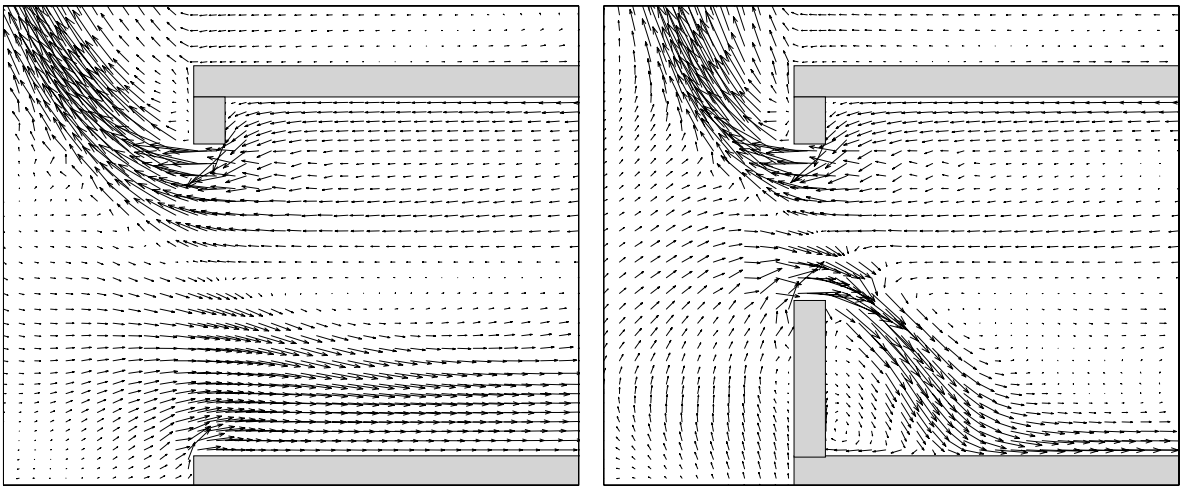

(a) Open door case (b) Open window case

Fig. 14 The mean air velocity distribution at the opening vicinity.